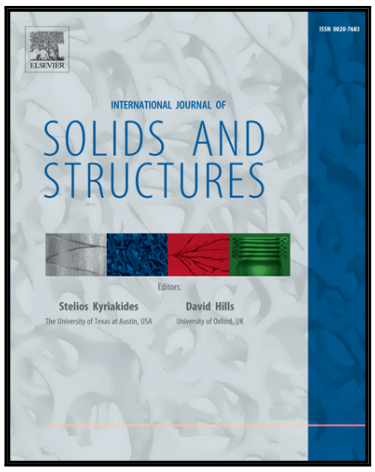

High fidelity modelling of the compression behaviour of 2D woven fabrics

Adam J. Thompson , Bassam El Said , Dmitry Ivanov , Jonathan P-H. Belnoue , Stephen R. Hallett

PII: S0020-7683(17)30293-7
DOI: 10.1016/j.ijsolstr.2017.06.027
Reference: SAS 9634

To appear in: *International Journal of Solids and Structures*

Received date: 3 October 2016
Revised date: 20 April 2017
Accepted date: 22 June 2017

Please cite this article as: Adam J. Thompson , Bassam El Said , Dmitry Ivanov , Jonathan P-H. Belnoue , Stephen R. Hallett , High fidelity modelling of the compression behaviour of 2D woven fabrics, *International Journal of Solids and Structures* (2017), doi: 10.1016/j.ijsolstr.2017.06.027

High fidelity modelling of the compression behaviour of 2D woven fabrics

Adam J. Thompson[1], Bassam El Said[1], Dmitry Ivanov[1], Jonathan P-H. Belnoue[1], Stephen R. Hallett[1]

[1]Advanced Composite Centre for Innovation and Science, University of Bristol, UK

*corresponding author: adam.thompson@bristol.ac.uk

Abstract

This paper proposes a new method for predicting the compression behaviour of 2D woven fabrics during the consolidation phase of Liquid Composite Moulding processes. A kinematic, multi-chain beam finite element method is first used to simulate the evolution of the internal architecture of a 2D woven fabric during single and multi-layer compaction processes. A hyper-elastic constitutive model, based on the compressive response of a single yarn, is then proposed and implemented into a finite element framework for analysis of the mechanical loading of the dry fabric. This utilises as-woven fabric geometries generated by the kinematic models, thus enabling predictions to be independent of detailed geometric and mechanical characterisation of physical fabric specimens. The model's ability to predict both the kinematic and mechanical response of the fabric, under compressive loads, is assessed by comparing the model outputs with X-ray Computed Tomography (CT) scans and the experimentally measured compaction response.

1. Introduction

Over the past 20 years, fibre reinforced composites have become key for applications where high stiffness to weight ratio is a driving parameter of design. Whilst their performance has been proven through recent commercial aircraft programmes, the main factor limiting their rapid growth is the long production times and associated high material and manufacturing costs. Liquid composite moulding (LCM) processes have played an integral role in facilitating growth in high-volume production industries, such as automotive, and are now being exploited in the aerospace sector to cope with the increasing rate of demand for commercial aircraft. This has increased the requirement for better predictability

of LCM processes to help ensure that the high consistency and quality required in aerospace, for both mechanical properties and dimensional tolerances, is maintained.

LCM processes are characterised by the impregnation of a dry textile preform with a liquid resin and include rigid mould processes such as RTM (Resin Transfer Moulding) and flexible bagging processes such as VARTM (Vacuum Assisted RTM) and RIFT (Resin Infusion Under Flexible Tooling) (Searle and Summerscales, 2005). An essential part of these processes is the consolidation of the dry reinforcement material to achieve the required fibre volume fraction. During this process the internal architecture of the reinforcement material is susceptible to large structural changes as it is forced to deform to allow for the reduction in its volume. These deformations can have significant effects on the mechanical performance of the final component and can make their final thickness, and subsequently their fibre volume fraction, difficult to predict.

The mechanistic analysis of the compressibility of fibrous structures has been the focus of a substantial amount of research which can be traced back to Van Wyk (1946) and his pioneering work on the compressibility of randomly orientated fibres. Van Wyk attempted to simulate the mechanics of fibre interaction by modelling them as a series of bending units. Assuming that fibre bending was the only relevant deformation mechanism, he was able to derive a relation between pressure and volume fraction of stochastically placed fibres. Later on, Gutowski (1992) developed a similar method with specific application to composite reinforcements. Many works which followed focused on modifying these relationships to account for other important mechanisms to gain higher accuracy (Komori and Itoh, 1997; Komori and Makishima, 1977; Pan, 1993).

More recent efforts (Alkhagen and Toll, 2007; Durville, 2005; Langston et al., 2015) have adopted methods traditionally used for the simulation of granular solids, where each of the fibres is represented as a slender particle and the compressibility is determined by the motion of inter-particle contacts and the resulting forces. Although fundamental, these methods are currently confined to the simulation of uni-directional and randomly orientated fibrous structures and are unable to deal with the computational requirements of woven textiles where single unit-cells typically contain several thousands of fibres. This currently limits their use for LCM processes which routinely use woven, braided and stitched structures.

One of the main difficulties for predicting the compressive response of woven textiles is their multi-scale nature. Typically, their micro-scale behaviour is determined by the

interactions of thousands of aligned fibres, bundled together to form yarns. These yarns are woven together to form complex, ordered, meso-scale structures, the behaviour of which is driven by the inter-yarn interactions as well as the fibre interactions within the yarns. As the meso-scale structure of woven fabrics has shown to affect both the permeability and the mechanical behaviour of the final component, it is necessary to predict the deformations of the structure as well as its compressive response.

The multi-chain group of methods has been one of the major breakthroughs in the discrete modelling of fibres within woven structures (Green et al., 2014; Mahadik and Hallett, 2010; Zhou et al., 2004). These methods are based on the discretisation of yarns into multiple 1D element chains, with each element chain representing a bundle of fibres. The interactions between the element chains during weaving and compaction processes is simulated through the use of contact models. Recent studies (El Said et al., 2014; Green et al., 2014) have shown the ability of these methods to capture both yarn cross-section deformation and yarn path evolution for 3D woven structures during the compaction process, achieving good correlation with x-ray micro-computed tomography (CT) scans. However, the kinematic nature of these methods limits their ability to determine the mechanical response of the fabric, as the properties of the physical constituents are not fully preserved within the model.

A second widely used set of methods consists in the homogenisation of the behaviour of the micro-scale structure within individual tows, via direct measurements, and focuses purely on the meso-scale inter-yarn interactions. Based on the assumption that the inter-tow contact is equal to the full width of the tow, Lomov and Verpoest (2000) generated an analytical model for the compressibility of a woven fabric. By using tow compressive and bending properties as well as other deformation modes as model inputs, the compacted fabric geometry is derived by minimising the bending energy of interlacing tows. A similar energy based method was also proposed by Potluri and Sagar (2008) to model the compressibility of multi-ply nested and 3D woven preforms.

Nguyen et al. (2013) analysed the compressive behaviour of multiple layers of a carbon fibre twill weave fabric by implementing a hypoelastic constitutive yarn model into a commercial finite element (FE) software package. The material parameters needed by the model were extracted through an inverse method on data obtained from a compaction test performed on a single layer of fabric. Predictions showed good agreement for the

compression of sheared and nested preforms. With the use of the inverse method reducing the requirement for accuracy of the internal architecture of the fabric.

Naouar et al. (2014) used a similar method to analyse the importance of an accurate representation of the initial fabric geometry for the prediction of the compressive behaviour of a 2/2 twill weave fabric. A comparison between FE models generated through TexGen (a textile modelling software) and models extracted directly from X-ray tomographic imaging was performed. Results showed that the X-ray tomography generated FE model, which considers the full non-idealised geometry of the fabric, leads to better predictions for both final geometry and compaction response.

The present study brings together two modelling techniques, implemented into a two-step modelling framework, that capture the multi-scale nature of textile reinforcement compaction. This framework allows multiple layers of fabrics and their interactions to be simulated using basic geometric data of the fabric architecture and a single yarn compaction curve. The first step utilises a kinematic, multi-chain method for generation of the initial as-woven geometry of the fabric. The second step uses this geometry to generate a 3D finite element model, able to capture both the kinematic and mechanical response of fabrics during compressive loading. The key benefit of this method is that the dependency on detailed geometric and mechanical examination of the physical specimen is removed. Hence, the possibility of making accurate predictions without access to the physical specimen is attained.

Considering a densely woven 2/2 twill weave fabric as an example, the first part of the paper focuses on the kinematic behaviour of the interlaced yarns during compaction. A multi-chain method for 2D fabrics is developed, based on (Green et al., 2014) to predict as-woven and compacted single and multi-layer fabric geometries. The fidelity of the method in capturing the kinematic behaviour of fabrics during compressive loading is examined and compared to X-ray micro-CT scans. The geometric features of the as-woven fabric, predicted by the kinematic method, are then used as an input for the 3D finite element analysis of fabric compaction. A constitutive relation linking the pressure applied on the yarn to its volume fraction is formulated within a hyper-elastic framework and implemented within a user material for the finite element package Abaqus. The model's ability to capture both the mechanical and kinematic behaviour of fabric during compaction processes is examined for both single and multi-layered preforms.

2. Kinematic Modelling of weaving and consolidation process

As discussed in the introduction, the compressibility of woven reinforcements is strongly determined by their internal architecture. Both the topology of the weave and the geometry of the individual yarns need to be considered. Multi-chain methods have been shown to provide good predictions for the deformation of the internal structure of fabrics during weaving and compaction processes.

In this section, a method initially proposed for 3D woven fabrics (Green et al., 2014) is adapted for 2D woven fabrics. The method's ability to capture the complex interactions during weaving and compaction processes is studied in more detail.

2.1 Method

As in Green et al. (2014) it is proposed here to represent each yarn within the fabric as a bundle of beam element chains. Each chain of elements is designated a circular cross section, whose area is determined by the number and the cross-sectional area of the fibres it represents. To capture the interaction between the element chains, during weaving and compaction processes, a general contact definition is applied to the model.

The bending behaviour of fibrous tows is an important property to consider in the deformation mechanics of textiles. Unlike conventional solid materials, their flexural stiffness is significantly lower than the tensile stiffness along the fibre direction. This is due to the low cohesion between the individual fibres, which allows for large relative displacements to occur. To capture tow bending effectively in the model, the beam element chains are given an elastic, perfectly plastic material behaviour to approximate the tow bending behaviour as plastic yielding. This methodology has been used in a number of studies (Mahadik and Hallett, 2010, Green et al., 2014, El Said et al, 2014) and the material properties, considering a 12k tow reduced to 61 beam element chains, have been tailored in Green et al. (2014) specifically to give a more realistic bending response. In that study, the 12k:61 fibre-to-beam element ratio was found to give the best compromise between accuracy and computational efficiency.

The process of building the models, including the application of the boundary conditions, material properties, element connectivity etc. has been implemented into a MATLAB subroutine which allows the generation of a range of traditional 2D fabrics. The output of this subroutine is an input file for LS-DYNA explicit finite element solver.

Initially a unit cell of a loose fabric topology is generated based on the kinematics of the weaving process. In order for the unit cell geometry to remain periodic throughout the weaving and compaction process, periodic boundary conditions are applied to the model. These periodic constraints are applied by connecting yarn end nodes, using Multi Point Constraints (MPC), which set restrictions on the mutual displacement of linked nodes.

As the loose fabric geometry results in the yarns having a longer length within the unit cell than the real fabric, the simulation begins by contracting the beam elements using an artificial coefficient of thermal expansion (CTE) for the material and applying a negative thermal load. This is equivalent to applying yarn tension during the weaving process, drawing the fabric together. The as-woven geometry is reached when the yarns achieve a state of equilibrium and hence the final yarn length is controlled by the interlacing of the yarns. Following this, compaction of the as-woven geometry can be performed by compressing it between two parallel rigid plates to the required thickness.

2.2 Single Layer Compaction

The ability of the proposed multi-chain method to capture the evolution of the internal architecture during the compaction of a single layer is assessed in this section. A 2/2 twill weave fabric was chosen for the analyses. Both the warp and weft yarns of this weave contain 12000 fibres, each fibre having a diameter of 7 μm, these are then woven into a fabric with a unit cell size of 9.5 mm^2 and an areal density of 660 g/m^2.

To begin with, a loose fabric topology was established, based on the fabric information provided above. A total of 61 beam element chains were used to represent each yarn, this number has shown to provide the best compromise between accuracy and computational efficiency (Green et al., 2014). The as-woven state was achieved by applying a thermal load to both the warp and the weft yarns. The obtained geometry was then compacted between two parallel plates, achieving the final compacted geometry. Figure 1 shows the evolution of the geometry of the model from loose topology to the compacted state. The geometry was extracted for further analysis at three stages: as-woven, compaction to 55% volume fraction (Vf) and compaction to 60% Vf.

To analyse the results the centrelines and surface geometries of each yarn were extracted from the multi-chain model following the methodology outlined by Green et al. (2013). Results were analysed in terms of intra yarn Vf, which represents the volume of fibres which lie within each yarn. The yarn paths were also analysed to determine the degree

of out of plane orientation (crimp) the yarns exhibit at each level of compaction. This was done by dividing the yarn centerlines along their length into multiple sections. Each section's local angle of deviation from a horizontal datum was calculated to provide a clear picture of the distribution of crimp the yarns exhibit at each level of compaction.

The as-woven geometry in Figure 2b shows the crimp angle gradually increasing along the length of the yarn up to the warp weft cross over sections. The intra-yarn Vf shown in Figure 3 varies significantly between each yarn.

When the fabric is compacted to 55% Vf the percentage of yarns with a crimp angle below 4° is significantly increased (Figure 2a). A length between yarn cross-over sections, with negligible out of plane orientation and no curvature, is generated. As the mean curvature along the length of the yarn reduces there are localised areas of high curvature induced, where the crimp angle is increased, due to the interactions between yarns at the warp/weft cross over regions. This results in an increase in the portion of the yarn with higher crimp angles (i.e. above 12°). In comparison to the as woven state, the intra-yarn Vf has become more uniform overall and has increased substantially. Localised areas of high and low Vf are evident due to the interaction between yarns at the cross-overs, constraining them in regions and allowing for expansion in others.

As the model is compacted further to 60% Vf this behaviour continues. The yarn cross over regions show a locally increased crimp angle, however the majority of the yarns' out of plane orientation is reduced. Localised areas of high intra-yarn Vf's are amplified but overall intra-yarn Vf seems not to have changed significantly.

2.3 Multi-Layer Compaction

For multi-layer woven fabric preforms one of the most important contributions to compaction is the nesting and packing of layers. Nesting, which occurs when successive layers are offset, alters the contact surface between layers, changing the compressive response of the fabric and the resulting deformations. No nesting was considered in the previous section as only a single layer was modelled. In this section, a shifted configuration, where successive plies are offset is analysed and compared to micro CT scans to see the accuracy of the model in predicting the evolution of the geometry during compaction.

One of the challenges in modelling offsets between layers is that the unit-cell of the fabric no longer remains constant from layer to layer, creating regions where yarns fall

outside the unit cell, thus compromising the periodicity of the model. In order to combat this issue, slave yarns are introduced. Slave yarns are placed outside the unit cell and mimic the behaviour of a yarn which lies within the unit cell at its opposing side. This is achieved by copying the yarns which lie at the edges of the unit cell (master yarns) and translating them by one unit cell length to their opposing side as shown in figure 4. Each node of the slave yarn is then fixed to the node it is a duplicate of within the master yarn in all 6 degrees of freedom using MPCs. This generates a contact surface for yarns within the layer as well as adjacent layers, hence maintaining the periodicity.

The offsets used in the model were determined using measurements from X-ray CT scans of an infused sample, manufactured through RTM. This ensured that realistic offsets were applied as well as allowing for validation of the final predicted geometry. An initially loose geometry was modelled of each layer within the shifted configuration, tension was then applied to each yarn simulating the weaving process. This was then followed by compaction of the stack between two parallel plates to a thickness corresponding to 55% Vf.

A comparison of the final predicted geometry to X-ray CT scans is illustrated in figure 5. The method appears to generate accurate predictions for both yarn path and yarn cross sectional shape. Both the interactions of the yarns within a layer and the effects of multiple layer stacking are captured, showing good agreement with the X-ray CT results.

Figure 6 shows the final distribution of intra yarn Vf in the shifted configuration compared with a perfectly aligned configuration for the same overall volume fraction. Although the magnitudes of intra-yarn Vf are similar in both models, the variation from layer to layer in the shifted configuration is significantly different as, unlike the aligned configuration, the contact surfaces between each layer varies. This results in a different compressive response, which has been observed in (Nguyen et al., 2013; Potluri and Sagar, 2008), and different locations within the unit cell for areas of high intra-yarn Vf.

3. Mechanical Modelling of Consolidation Process

The kinematic models in the previous section were able to predict the evolution a fabric architecture during consolidation. Although this kinematic behaviour does have an effect on the performance of the final composite, another key variable is the global fibre volume fraction. For woven fabrics, the volume fraction at a given pressure depends on the design and density of the weave architecture, with the maximum achievable volume fraction varying between fabrics. Therefore to model LCM processes, which are typically pressure controlled,

a model must be able to capture both the kinematic and mechanical response of the fabric in order to be fully predictive.

Although the multi-chain method is capable of generating the geometry of fabric to a good degree of accuracy, it is limited in predicting their mechanical response. This is a result of three key aspects of the model. Firstly, there is the use of an elasto-plastic material behaviour, which has been pragmatically tailored to capture the deformation of the fabric architecture, rather than the local mechanical behaviour of the fibres. Secondly, the nature of 2D beam elements does not allow for cross-section consolidation and thus the compressibility of the textile is limited by the cross-sectional area of the beams. Finally, the mechanical response of textiles, at the meso-scale, is dominated by the interactions of the individual fibres, with inter-fibre friction being a key property. The diameter of a single beam element chain, which represents a bundles of fibres, is calculated using the sum of the cross sectional areas of the fibres they represent, and hence, the surface area of the fibres is not explicitly represented. To include accurate friction behaviour in the model, the true surface area of the fibres would have to be present. This could be possible by increasing the number of beam element chains closer to the number of fibres present in the yarn structure, however, the computational expense in doing so would be substantial and would result in unfeasibly long run times.

A method is therefore proposed here, whereby, the detailed as-woven geometry generated using the multi-chain element method is extracted and meshed with solid hexahedral elements. An experimentally determined compaction curve of a single yarn is used to deduce a relationship between intra-yarn volume fraction and pressure. Combining this relationship with the as-woven geometry enables the initial transverse stiffness for each yarn to be determined and updated incrementally based on the volumetric strain. By implementing this relationship into a hyper-elastic framework (applied within a user defined material subroutine in the FE package Abaqus) the compressibility of the yarns is handled by the constitutive relationship and the overall compressive response of the fabric, resulting from the interaction of interlacing yarns, is handled through the application of contact models.

3.1 Hyper-Elastic Framework

The high transverse compliance of fibre bundles is such that any constitutive model aiming at capturing the mechanical behaviour of yarns needs to be built into a large deformation framework. Multiple studies (Charmetant et al., 2012; Charmetant et al., 2011; Naouar et al., 2015) have implemented hyper-elasticity into material models to capture the large rotations of the fibre direction experienced during complex loading of interlacing yarns. The use of hyper-elasticity assumes that the deformation behaviour of a fibrous mass is fully reversible, which is not strictly true as observed in (Bickerton et al., 2003; Ivanov and Lomov, 2014). However, the compressive loading in LCM processes is generally defined as being monotonic and hence, the non-reversible behaviour can be approximated by a reversible model (Nguyen et al., 2013).

It is assumed here that the yarn behaviour can be described through continuum solid elements. The material is assumed to be transversely isotropic. A unit vector, $\boldsymbol{n}_0$, locally defines the fibre direction of the material (Spencer, 1984). The hyper-elastic definition builds on the work of Bonet and Burton (1998) who formulated a hyper-elastic strain energy function for transversely isotropic materials as shown in equation 1.

Equation 1

$$\psi = \frac{1}{2}\mu_T(I_1 - 3) - \mu_T \ln(J) + \frac{1}{2}\lambda(J-1)^2 + \left[(\mu_T - \mu_L) + \frac{\alpha}{4}\ln(J) + \frac{\beta}{8}(I_4 - 1)\right](I_4 - 1) + \frac{1}{2}(\mu_T - \mu_L)(I_5 - 1)$$

where ψ is strain energy potential and $\boldsymbol{I}_1, \boldsymbol{I}_2, \boldsymbol{I}_3$ are the standard invariants for isotropic materials and in this case describe the isotropy present in the frame orthogonal to the fibre direction. The final two invariants $\boldsymbol{I}_4, \boldsymbol{I}_5$ provide a measure of the strain in the principle fibre direction. The material parameters are determined using a linearization procedure, as discussed in (Latif et al., 2007), which allows $\lambda, \alpha, \beta, \mu_T$ and μ_L to be expressed as functions of the engineering constants by equations 2-7.

Equation 2

$$\lambda = \frac{v_T + {v_L}^2}{E_L E_T \Delta}$$

Equation 3

$$\alpha = \frac{v_L + v_T v_L}{E_L E_T \Delta} - \lambda$$

Equation 4

$$\beta = \frac{2E_L - 4G_L - E_L E_T (1 - 2v_L)^2}{2\left(2E_T {v_L}^2 + E_L(v_T - 1)\right)} - \frac{E_T}{1 + v_T}$$

Equation 5

$$\mu_L = G_L$$

Equation 6

$$\mu_T = G_T$$

Equation 7

$$\Delta = \frac{1 - {v_T}^2}{E_L {E_T}^2}$$

The engineering constants are the Young's modulus E, the Shear modulus G, and the Poisons ratio v, the subscripts T (transverse) and L (longitudinal) define the material direction the constants belong to.

Under the assumptions that the behaviour is reversible, does not dissipate energy and fulfils the Clausius-Duhem inequality, the constitutive equation of a hyper-elastic material can then be expressed as:

Equation 8

$$\boldsymbol{S} = 2\left(\frac{\partial \psi}{\partial \boldsymbol{C}}\right)$$

where $\boldsymbol{S}$ is the second Piola-Kirchoff stress tensor. The elastic potential (ψ) depends on the position ($\boldsymbol{X}$) of the material point, the right Cauchy-Green deformation tensor ($\boldsymbol{C}$) and the structural tensor ($\boldsymbol{N}_0$) which characterises the local directional properties of the material and is defined as $\boldsymbol{N}_0 = \boldsymbol{n}_0 \otimes \boldsymbol{n}_0$.

3.2 Determination of elastic constants

During consolidation of aligned fibre bundles (yarns or tows) the gaps between the individual fibres are closed and the fibres are forced to rearrange through sliding and bending until the inter-fibre contacts fully constrain the fibrous network. This results in the compressive stiffness of the yarn increasing significantly as the intra yarn volume fraction approaches its upper limit. For a given yarn, the maximum intra-yarn fibre volume fraction (ϕ) achievable is difficult to determine as it is dependent on the alignment and distribution of the fibres. The maximum theoretically achievable ϕ is if the fibres are perfectly aligned and pack into an ideal hexagonal formation, which would give a packing factor of 0.907. However, this is likely to be unachievable due to entanglement, misalignment, slight twisting of yarn bundles, and non-uniform distribution of fibres in the initial configuration. Gutowski et al. (1987) stated that the maximum available fibre volume fraction limit for aligned fibres laid between square and hexagonal packing i.e 0.785-0.907.

A compaction curve of a single yarn, taken from the 2/2 twill weave detailed in section 2.2, is presented in figure 7a. The yarn studied was a 12k carbon fibre yarn with 7µm fibre diameter. The approximate width of the yarns was 2.6mm. The graph shows the typical behaviour of a fibrous network where the compressibility of the yarn is reduced with increased pressure until the yarn reaches maximum compaction. Assuming the yarn spread is negligible, which was observed in (Ivanov and Lomov, 2014) and reinforced further in (Latil et al., 2011), a relation between fibre volume fraction and pressure can be deduced. The compaction pressure-fibre volume fraction relationship is presented in figure 7b which shows the yarn to stiffen as the volume fraction increases.

To represent this stiffening effect, induced by the increased inter-fibre contacts, the yarn is modelled as a non-linear transversely isotropic material where the transverse modulus is updated incrementally based on the total volumetric strain of the element. The increase in the modulus simulates the fabric getting stiffer as the volume fraction is increased. As the yarns within the fabric geometry have varying magnitudes of ϕ along their length (as shown in figure 3), the compressibility along their length will also vary. To account for this, the intra yarn volume fraction at the current time step is determined by equation 9, where ϕ_i is the initial intra yarn volume fraction and $detF$ is the determinant of the deformation gradient.

Equation 9

$$\phi_n = \phi_i / detF$$

The transverse Young's modulus, E_T, of the yarn at each stage of compaction can then be derived from figure 7b and updated incrementally. This is the fundamental parameter behind this constitutive model where the transverse shear modulus, G_T, is determined using the basic material constant definition in equation 10.

Equation 10

$$G_T(\phi_n) = \frac{E_T(\phi_n)}{2(1+v)}$$

As the magnitude of the yarn spread was observed to be negligible the poison ratio, v, is assumed to be zero. The Young's modulus, E_L, along the fibre path is significantly higher than the transverse direction and is updated incrementally based on ϕ_n, using the basic rules of mixtures in equation 11.

Equation 11

$$E_L(\phi_n) = E_f \phi_n$$

where E_f is the Young's modulus of the individual fibres. The bending stiffness of the yarn, like the transverse stiffness in tension, is very low due to the low cohesion between the individual fibres, allowing for relative inter-fibre slippage to occur. This is represented within the model by assigning a very low shear modulus along the fibre path, following (Boisse et al., 2005).

This definition of the elastic constants results in a model that has three strain dependent moduli: E_T, G_T and E_L. For these to be represented correctly in the hyper-elastic framework, presented in section 3.1, an updated Lagrange procedure needs to be implemented to update the stress variables incrementally (Nagtegaal and De Jong, 1981). This step is vital to ensure the full strain history is captured correctly. Therefore, the second Piola-Kirchoff stress at the current time step, n, is determined by equation 12.

Equation 12

$$\boldsymbol{S}^n = \boldsymbol{S}^{n-1} + \Delta \boldsymbol{S}(\phi_n)$$

where $\Delta \boldsymbol{S}(\phi_n)$ is the increment in the second Piola-Kirchoff stress found through the incremental constitutive relation between the Lagrangian elasticity tensor, $\mathbb{C}$, and the Right Cauchy-Green strain increment, $\Delta \boldsymbol{E}$, presented in equation 13.

Equation 13

$$\Delta \boldsymbol{S}(\phi_n) = \mathbb{C}(\phi_n) : \Delta \boldsymbol{E}$$

The elasticity tensor relates the Piola-Kirchoff stress to the Right Cauchy-Green strain tensor and is fully non-linear. The expression for $\mathbb{C}$ follows Holzapfel et al. (1996) and is given in (Bonet and Burton, 1998).

3.3 Geometry Extraction and Meshing

To apply the hyper-elastic constitutive model to yarns within a fabric, a detailed and accurate description of both the yarn geometry and fabric topology is required. Here, the as-woven geometry is generated using the multi chain element method discussed in section 2. There are two motivations behind choosing this method for initial geometry generation. Firstly, the geometry of the yarns within a fabric is directly related to the topology of the weave. As the multi-chain method generates the geometry based on the interaction of the yarns, the change in cross section and hence ϕ along the yarns length is correctly captured through the interlacing and contact of the yarns. Secondly, the geometry generation requires minimum input parameters, which are readily available from the fabric data sheet, allowing the method to be a powerful pre-processor for geometry generation.

In generating the as-woven geometry using this method the surface geometry of the yarns needs to be extracted and meshed as solid entities. To do this the nodal coordinates of the as-woven geometry must first be extracted. The yarn paths and cross-sections of each yarn are then extracted following the method proposed by Green et al.(Green et al., 2013). Here the yarn centrelines are described by a one dimensional line in three dimensional space and the yarn-cross sections are defined by two-dimensional shapes on planes perpendicular to the yarn centreline. Multiple cross-sections define each individual yarn to ensure the full fidelity of the multi-chain geometry is captured.

The points defining each cross-section are then redistributed uniformly to allow for the yarn cross-sections to be discretised into quadrilaterals. The new, uniformly distributed points are then defined as nodes and nodal connectivity is prescribed to generate a structure of hexahedral elements, accurately representing the as-woven geometry generated from the

multi-chain method. The before and after results of this process for the 2/2 twill weave discussed in section 2 is illustrated in figure 8.

During this meshing process the volume fraction (ϕ_n) and the fibre direction ($\boldsymbol{n}_0$) for each section along the length of each yarn is calculated and passed to the material model. The calculation of both of these parameters is performed under the assumption that the fibres in each yarn section are parallel and evenly distributed across the transverse plane of the section. A pre-processor, allowing for the geometry extraction, meshing and building of an input file for the commercial FE package Abaqus Explicit (which includes material assignments and periodic boundary conditions), was built using Matlab.

3.4 Single Layer Compaction

A simulation of the transverse compaction of a single layer of the 12k, 2/2 twill weave fabric was performed. The model parameters are presented in Table 1. Where the second order exponential expression defining the transverse modulus of the yarns was derived from the ϕ/pressure relationship shown in figure 7b. Periodic boundary conditions were applied by constraining the yarn end nodes' degrees of freedom to move with their relative node on the opposing end of the yarn. The model was then compacted between two parallel rigid surfaces.

Table 1 – Model input parameters

E_F (MPa)	E_T (MPa)	G_L (MPa)	v	A	B	C	D
240	$Ae^{B\phi_n} + Ce^{D\phi_n}$	10	0	6.29E-4	11.72	5.38E-19	54.59

Figure 9 shows the change in intra yarn volume fraction from as-woven to maximum compaction. As stated above, the as-woven intra yarn volume fraction is initially assumed to be constant across the width of the yarn for each cross-section, but varies along the length of the yarn due to the interlacing of the yarns. When the geometry is compacted the distribution and magnitude of the intra yarn volume fraction changes depending on the constraints applied by the contacting surfaces. Any increase of the local intra yarn volume fraction ultimately leads to an increase of the compressive stiffness of that element.

To determine the accuracy of the proposed method, compaction experiments were performed on 5 samples of the same fabric as modelled here for comparison. Each sample was a 100mm^2, single layer of the 2/2 twill weave. The samples were placed on the bottom

plate of a 10kN load cell universal testing machine and compacted at a rate of 0.5mm/min. The machine compliance was measured prior to the test and the nonlinear machine displacement was subtracted from the measured displacements in the post-processing of the results.

Figure 10 shows the comparison between experimental and predicted compaction loads. Generally, good agreement between the model predictions and the experimental data is obtained. The discrepancies in volume fraction below 0.1MPa can be attributed to the differences in initial geometry and the approximation of the low bending stiffness of the yarns represented through an assumed value of transverse shear stiffness in the model. However, the differences are minor and for LCM processes, the state of fabrics at pressures above 0.1MPa is the main area of interest.

3.5 Multi-Layer Compaction

The developed model can be further used to consider the compaction of a stack of 6 layers, comparing the compressibility of the aligned and shifted configuration examined in section 2.3. As with the multi-chain method, the shifted configuration poses the problem of a non-constant unit cell through the thickness of the stack. To solve this, slave yarns were introduced into the model following the same method used for the multi-chain method. In this instance the elastic constants of the slave and master yarns were reduced by a factor of 2 to account for the cross-sectional area being effectively doubled by tying the slave and master yarn nodes together.

Comparing the 6 layer aligned configuration with the single layer in figure 11, it is evident that the curves converge at higher pressure. The lower stiffness exhibited in the 6 Layer aligned stack at pressures below 0.1 MPa can be explained, again by the area of the contacting surfaces. Each yarn in the single layer model is compressed between the rigid tool and the adjacent yarns. In the multi-layer model, the majority of the yarns are not in contact with the rigid tool and are only compacted by adjacent yarns. At low pressures the contact area between crossing yarns is significantly lower than the yarn/tool contact area. As the pressure increases the contact area of crossing yarns increases and the stiffness of the layup begins to converge with the single layer results.

The results for the shifted configuration are as expected. The nesting significantly increases the compressibility of the stack, enabling higher volume fractions to be achieved. This behaviour has also been observed in (Nguyen et al., 2013; Potluri and Sagar, 2008).

Considering the deformed geometry, figure 12 shows the finite element model is also able to capture the deformation behaviour of the yarns to a reasonable degree of accuracy. However, the comparison shows the area of the cross sections to be consistently smaller than both the experimental results and predictions made using the multi-chain method (figure 5). This is most likely due to the assumption of zero Poisson's ratio in the constitutive model (equation 10) and that the transverse expansion behaviour of a free yarn is representative of a yarn within a woven structure (Ivanov and Lomov, 2014).

4. Conclusions

A large part of the mechanical behaviour of fabrics is governed by the yarn and fibre interactions; with the use of contact models the multi-chain method is able to capture these interactions with minimum input requirements. It has been shown that this modelling technique is able to capture the deformation mechanisms that occur through compaction of single and multi-layered stacks of a densely packed 2/2 twill weave. Comparisons +with X-ray CT scans showed the method is capable of generating deformed fabric architectures with a high degree of accuracy, highlighting its potential as a powerful pre-processor for geometry generation.

In comparison to alternative methods for generating textile geometry for modelling purposes, the multi-chain method offers a good compromise between analytical methods and direct extraction from µCT scans. Analytical methods take minutes (or even seconds) to run, but generate idealised geometries, which may be subject to interpenetrations between yarns and have less realistic intra yarn fibre volume fractions and yarn paths. At the other end of the scale, geometry extraction from µCT data, where the accuracy is uncompromised, requires fabrication of the textile architecture, µCT imaging and then post processing. With the multi-chain element method, a single compacted layer of the 2/2 twill weave, presented in this paper, can be achieved in less than one hour, running on 4 CPU. The geometry can be extracted, and analysed at different stages of compaction with ease and can be utilised for stiffness and failure modelling of the textile composite and resin injection flow modelling. In the context of this work, the predicted as-woven geometry has been exploited for mechanical characterisation of the compressive behaviour of the dry textile.

A finite element-based method has been proposed to determine the mechanical response of the fabric during compaction. This coupled the as-woven geometry, generated by the multi-chain method, with a hyper-elastic yarn constitutive model. The constitutive model is

based on a relation between the intra yarn volume fraction and the compressive load applied to an individual yarn. This relation can be derived from a compression test on a single yarn. The procedure allows for the mechanical complexities of the fabric to be predicted using just basic dimensional information.

Results for the compaction load of a single layer of the 2/2 twill weave showed good agreement with experimental results. The compaction of multiple layers, considering configurations both with and without nesting, was also performed and showed the expected behaviour, which is consistent with literature. Comparisons with X-ray CT scans also show that the method is capable of capturing the deformed geometry of the yarns with good accuracy.

The main benefit of the proposed method is the non-dependency on physical geometric and mechanical examinations of the fabric. Predictions are made using basic geometric information, which is readily available from the fabric supplier, and a single yarn compression curve. Future work will focus on examining the robustness of this method, considering different weave architectures and yarn fibre counts, as well as examining the method to consider other modes of deformation.

Acknowledgements

This work has been funded by the EPSRC through the Doctoral Training Partnership (DTP) grant to the University of Bristol (EP/L504919/1) and the Centre for Innovative Manufacturing in Composites EPSRC project “Defect Generation Mechanisms in Thick and Variable Thickness Composite Parts - Understanding, Predicting and Mitigation” (DefGen), (EP/I033513). The authors would also like to acknowledge the contribution of Mikhail Matveev, from the University of Nottingham, for providing the X-ray CT scans used in this work.

References

Alkhagen, M.r., Toll, S., 2007. Micromechanics of a Compressed Fiber Mass. Journal of Applied Mechanics 74, 723.

Bickerton, S., Buntain, M.J., Somashekar, A.A., 2003. The viscoelastic compression behavior of liquid composite molding preforms. Composites Part A: Applied Science and Manufacturing 34, 431-444.

Boisse, P., Gasser, A., Hagege, B., Billoet, J.-L., 2005. Analysis of the mechanical behavior of woven fibrous material using virtual tests at the unit cell level. Journal of Materials Science 40, 5955-5962.

Bonet, J., Burton, A.J., 1998. A simple orthotropic, transversely isotropic hyperelastic constitutive equation for large strain computations. Computer Methods in Applied Mechanics and Engineering 162, 151-164.

Charmetant, A., Vidal-Salle, E., Boisse, P., 2012. 3D Hyperelastic Constitutive Model for Yarn Behaviour Description. Key Engineering Materials 504-506, 267-272.

Charmetant, A., Vidal-Sallé, E., Boisse, P., 2011. Hyperelastic modelling for mesoscopic analyses of composite reinforcements. Composites Science and Technology 71, 1623-1631.

Durville, D., 2005. Numerical simulation of entangled materials mechanical properties. Journal of Materials Science 40, 5941-5948.

El Said, B., Green, S., Hallett, S.R., 2014. Kinematic modelling of 3D woven fabric deformation for structural scale features. Composites Part A: Applied Science and Manufacturing 57, 95-107.

Green, S.D., Long, A.C., El Said, B.S.F., Hallett, S.R., 2014. Numerical modelling of 3D woven preform deformations. Composite Structures 108, 747-756.

Green, S.D., Long, A.C., Hallett, S.R., 2013. Simulated textile geometry with realistic deformations for finite element modelling, TexComp-11, Leuven.

Gutowski, T., Cai, Z., Bauer, S., Boucher, D., Kingery, J., Wineman, S., 1987. Consolidation experiments for laminate composites. Journal of Composite Materials 21, 650-669.

Gutowski, T., Dillon, G., 1992. The elastic deformation of lubricated carbon fiber bundles: comparison of theory and experiments. Journal of Composite Materials 26, 2330-2347.

Holzapfel, G.A., Eberlein, R., Wriggers, P., Weizsäcker, H.W., 1996. Large strain analysis of soft biological membranes: Formulation and finite element analysis. Computer methods in applied mechanics and engineering 132, 45-61.

Ivanov, D.S., Lomov, S.V., 2014. Compaction behaviour of dense sheared woven preforms: Experimental observations and analytical predictions. Composites Part A: Applied Science and Manufacturing 64, 167-176.

Komori, T., Itoh, M., 1997. Analyzing the compressibility of a random fiber mass based on the modified theory of fiber contact. Textile research journal 67, 204-210.

Komori, T., Makishima, K., 1977. Numbers of fiber-to-fiber contacts in general fiber assemblies. Textile Research Journal 47, 13-17.

Langston, P., Kennedy, A.R., Constantin, H., 2015. Discrete element modelling of flexible fibre packing. Computational Materials Science 96, 108-116.

Latif, M.A., Peric, D., Dettmer, W., 2007. Numerical Modeling of Transversely Isotropic Elastic Material at Small and Finite Strains, Solid State Science and Technology: The 2nd International Conference on Solid State Science and Technology 2006. AIP Publishing, pp. 142-146.

Latil, P., Orgéas, L., Geindreau, C., Dumont, P., Du Roscoat, S.R., 2011. Towards the 3D in situ characterisation of deformation micro-mechanisms within a compressed bundle of fibres. Composites Science and Technology 71, 480-488.

Lomov, S.V., Verpoest, I., 2000. Compression of Woven Reinforcements: A Mathematical Model. Journal of Reinforced Plastics and Composites 19, 1329-1350.

Mahadik, Y., Hallett, S.R., 2010. Finite element modelling of tow geometry in 3D woven fabrics. Composites Part A: Applied Science and Manufacturing 41, 1192-1200.

Nagtegaal, J., De Jong, J., 1981. Some computational aspects of elastic-plastic large strain analysis. International Journal for Numerical Methods in Engineering 17, 15-41.

Naouar, N., Vidal-Salle, E., Schneider, J., Maire, E., Boisse, P., 2015. 3D composite reinforcement meso F.E. analyses based on X-ray computed tomography. Composite Structures 132, 1094-1104.

Naouar, N., Vidal-Sallé, E., Schneider, J., Maire, E., Boisse, P., 2014. Meso-scale FE analyses of textile composite reinforcement deformation based on X-ray computed tomography. Composite Structures 116, 165-176.

Nguyen, Q., Vidal-Sallé, E., Boisse, P., Park, C., Saouab, A., Bréard, J., Hivet, G., 2013. Mesoscopic scale analyses of textile composite reinforcement compaction. Composites Part B: Engineering 44, 231-241.

Pan, N., 1993. A modified analysis of the microstructural characteristics of general fiber assemblies. Textile Research Journal 63, 336-345.

Potluri, P., Sagar, T.V., 2008. Compaction modelling of textile preforms for composite structures. Composite Structures 86, 177-185.

Searle, T.J., Summerscales, J., 2005. Low-pressure (vacuum infusion) techniques for moulding large composite structures. Proceedings of the Institution of Mechanical Engineers, Part L: Journal of Materials: Design and Applications 219, 45-58.

Spencer, A.J.M., 1984. Continuum theory of the mechanics of fibre-reinforced composites. Springer.

Van Wyk, C., 1946. 20—Note on the compressibility of wool. Journal of the Textile Institute Transactions 37, T285-T292.

Zhou, G., Sun, X., Wang, Y., 2004. Multi-chain digital element analysis in textile mechanics. Composites Science and Technology 64, 239-244.

Figure 1 – Multi-chain element model of 2/2 twill weave; initial loose topology (left), as-woven geometry (middle), compacted geometry (right)

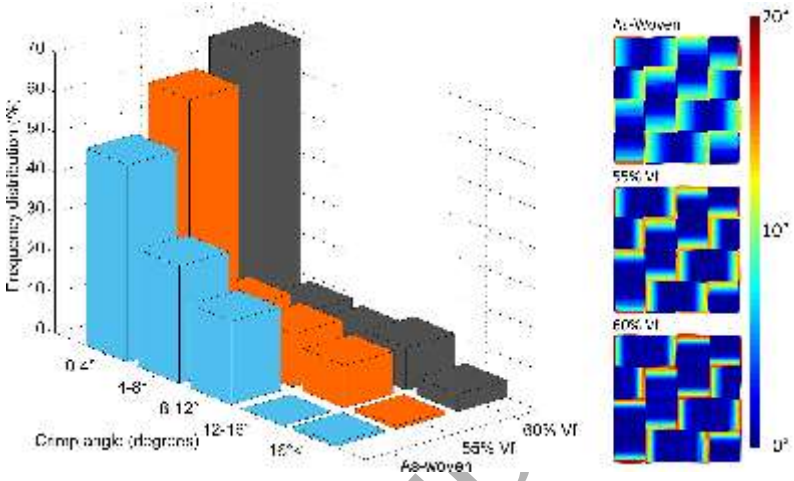

Figure 2 – a) Histogram showing the frequency distrubition of crimp angle at 3 stages of compaction b) Gradient plots showing the evolution of crimp angle (within the fabric) at 3 stages of compaction

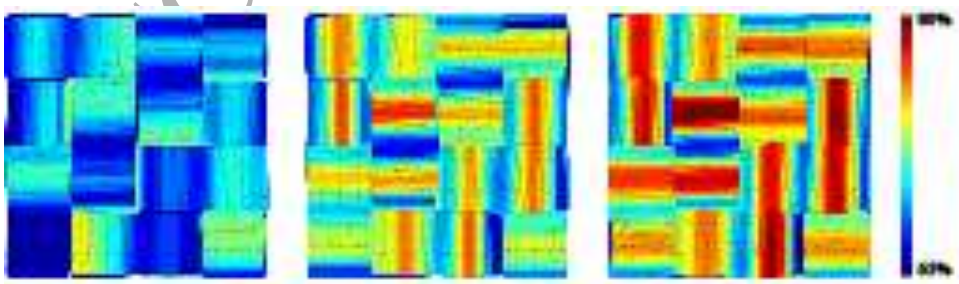

Figure 3 – Visualisation of the intra yarn Vf for as-woven (left), 55%Vf (middle), 60%Vf (right)

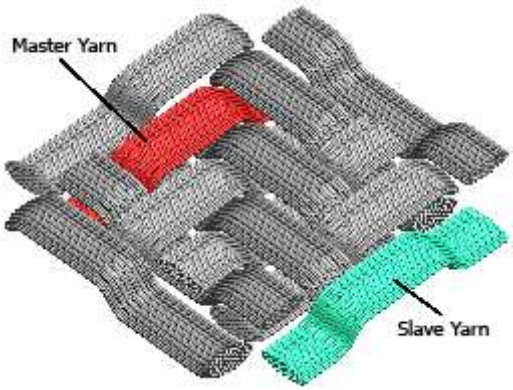

Figure 4 – Single layer unit cell with the addition of the slave yarns. Red highlighting a single master yarn and green is its corresponding slave yarn.

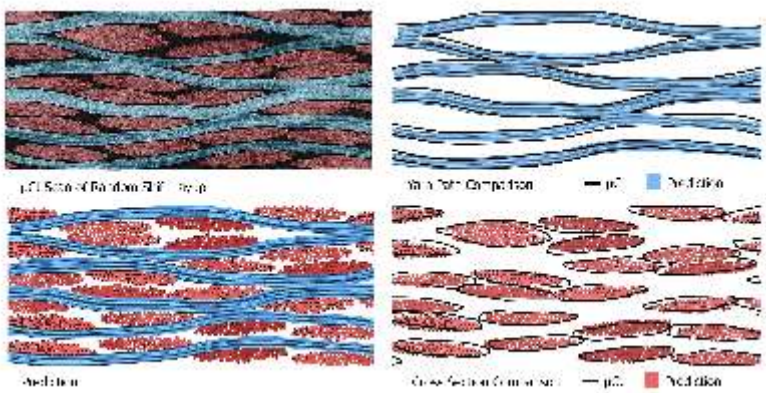

Figure 5 – Comparisons of the predicted yarn geometry with X-ray CT scans for 6 layer arbitrary shift stack

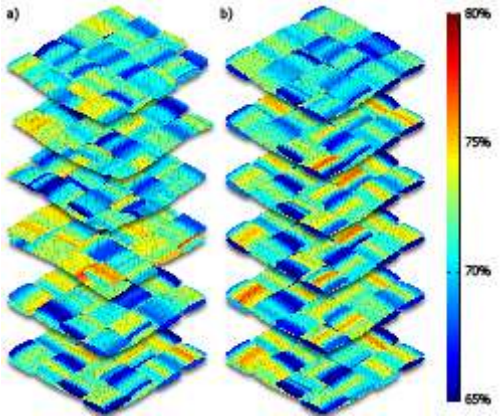

Figure 6 – Predictions for the distribution of intra yarn volume fraction for a) 6 Layer arbitray shift configuration and b) 6 layer perfectly aligned configuration

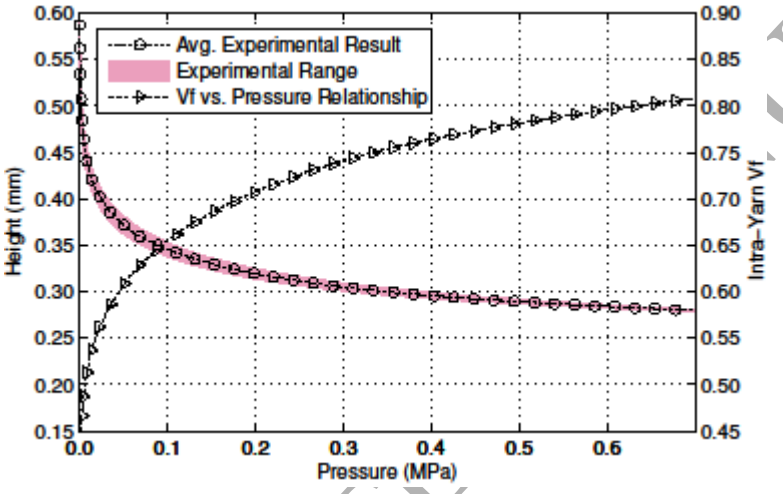

Figure 7 – a) Experimental results of a single yarn compaction test b) derived relationship of the intra yarn volume fraction/compaction load

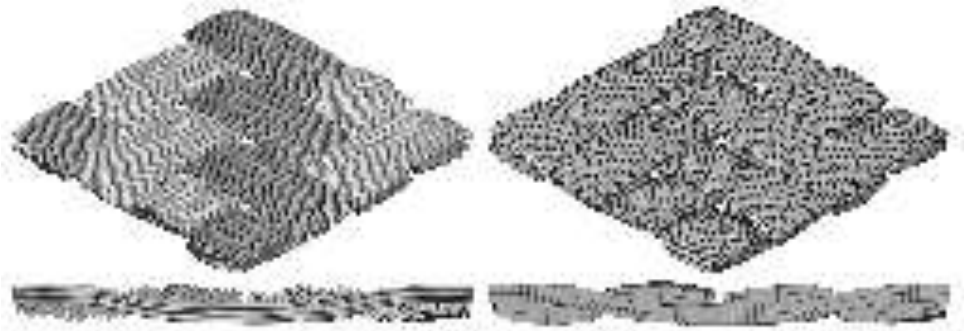

Figure 8 – As-woven multi-chain geometry of the 2/2 twill weave and the extracted geometry meshed with hexahedral elements

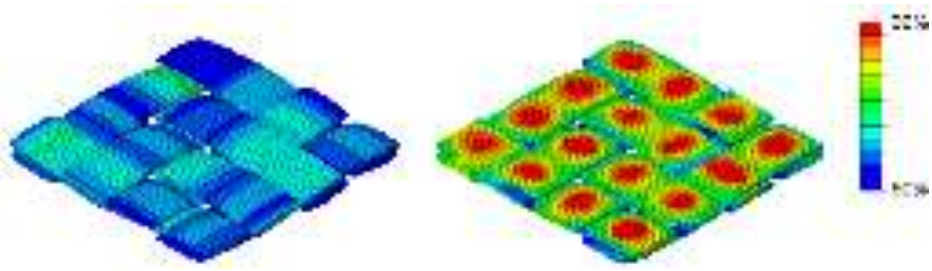

Figure 9 – Model results for the intra yarn volume fraction before (left) and after (right) compaction

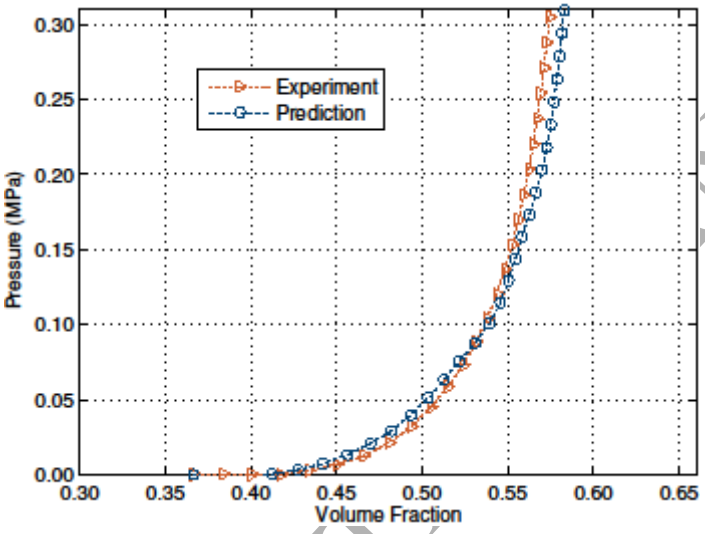

Figure 10 – Comparison between predicted and experimental results for a single layer 2/2 twill weave compaction

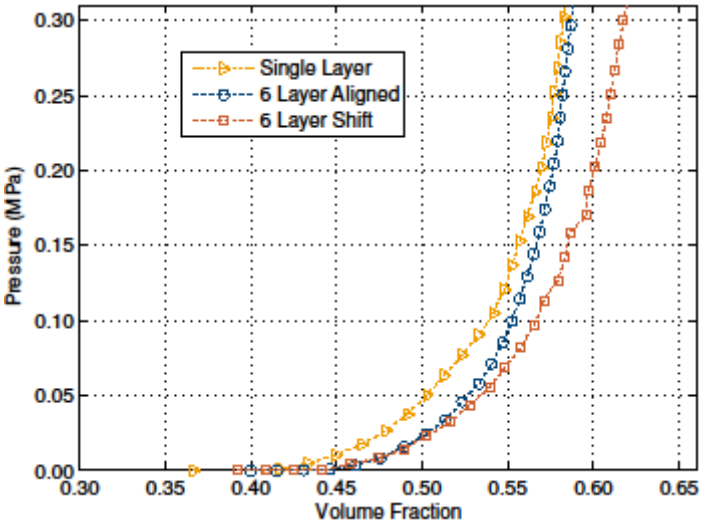

Figure 11- Comparison of a single layer compaction with a 6 layer compaction with and with-out nesting

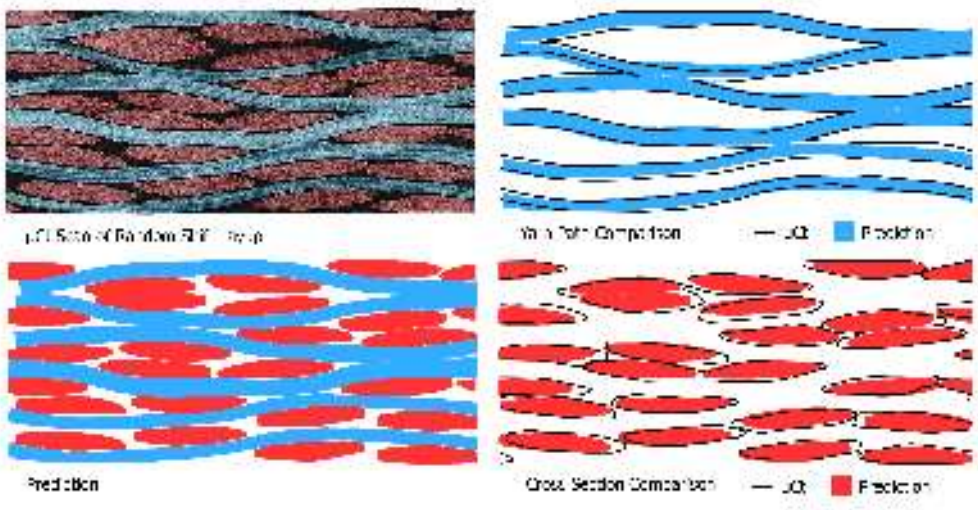

Figure 12 - Comparisons of the 3D FE predicted yarn geometry with X-ray CT scans for 6 layer arbitrary shift stack